Influence of *d* electrons on the dispersion relation of Ag surface plasmons for different single-crystal faces

Catalina López Bastidas and Ansgar Liebsch
Institut für Festkörperforschung, Forschungszentrum Jülich, 52425 Jülich, Germany

W. Luis Mochán
Centro de Ciencias Físicas, Universidad Nacional Autónoma de México, Apartado Postal 48-3, 62251 Cuernavaca, Morelos, Mexico
(Received 2 November 2000; published 2 April 2001)

The surface plasmon dispersion relation of Ag is calculated for different single-crystal orientations. To describe the dynamical response properties of both delocalized 5*s* electrons and more tightly bound 4*d* electrons, the jellium model is combined with the so-called dipolium model, in which the occupied Ag *d* bands are represented in terms of polarizable spheres located at the sites of a semi-infinite fcc lattice. The nonlocal susceptibility characterizing the *s* electron response in the surface region is derived using density functional theory. The screening of the Coulomb interaction between conduction electrons via the lattice of dipoles, and of the dipole interaction via the surrounding sea of conduction electrons, is treated self-consistently. Electron energy loss spectra are calculated for all three low-index faces. The surface plasmon energy is found to increase with parallel wave vector for all cases. The magnitude of the positive slope depends on the crystal orientation and, for Ag(110), on the propagation direction. These results are in qualitative agreement with electron energy loss measurements.

DOI: 10.1103/PhysRevB.63.165407 PACS number(s): 73.20.Mf, 78.20.Ci

I. INTRODUCTION

The spectroscopic characterization of surfaces is of interest both from a basic theoretical and practical point of view. On the one hand, electronic excitations at surfaces reflect the microscopic electronic and structural properties in the surface region and the response to external electromagnetic fields.[1–3] On the other hand, the sensitivity of surface collective excitations to surface conditions, e.g., at metal-electrolyte interfaces, has recently been utilized with great success in methods such as surface plasmon spectroscopy, for the purpose of developing efficient and robust chemical and biological sensors.[4] Noble metals are among the most thoroughly investigated systems in basic surface science. They are also particularly interesting for practical applications.

A central quantity to study is the variation of the surface plasmon and plasmon-polariton excitation energy with parallel wave vector $q_\parallel$. In the case of Ag, electron energy loss measurements[5–7] showed that the dispersion relation of surface plasmons differs in several important ways from that observed on simple metals.[8–11] In the nonretarded small $q_\parallel$ limit, the frequency strongly disagrees with the relation[12] $\omega_s = \omega_p/\sqrt{2}$, where ω_p is the bulk plasma frequency. At finite $q_\parallel$, the Ag surface plasma frequency increases, whereas on simple metals the frequency first diminishes and only beyond $q_\parallel \approx 0.15$ Å^{-1} increases. Finally, the positive slope of the dispersion differs appreciably for the three low-index crystal faces of Ag while lattice effects are negligible on simple metals. Evidently, the presence of the shallow occupied *d* bands has a profound influence on the overall frequency and momentum dispersion of the Ag surface collective excitations.

Theoretical studies including *s* and *d* bands have been carried out only recently for the optical properties of Ag bulk[13] and thin films.[14] A dynamical treatment of the surface screening response including the full Ag band structure is computationally not yet feasible. For this reason, various simplified models have been developed in the past with the aim of describing some of the observed features of Ag surface plasmons.[15–19] In one of these approaches[17,18] the emphasis is on the microscopic description of the nonlocal response of the *s* electrons in the surface region, while the influence of the *d* bands is qualitatively included via a semi-infinite polarizable medium. In this scheme, the Ag surface plasma frequency in the long wavelength limit $\hbar\omega_s^* = 3.7$ eV, and the overall positive slope at finite $q_\parallel$ can be understood in simple physical terms. Lattice effects, however, such as the dependence of the dispersion on crystal orientation, are absent in this model. A complementary approach[15,16] focuses on the dynamical response of *d* electrons, representing them via a semi-infinite fcc lattice of polarizable point dipoles. A local Drude model was used to describe the influence of the surrounding *s* electron gas. While crystallinity effects are included naturally in this ''dipolium'' scheme, the profile of the conduction electron density near the surface is approximated and its nonlocal response properties are neglected.

The aim of the present work is to combine the attractive features of these two approaches in order to arrive at a more realistic description of the Ag surface plasmon dispersion with parallel wave vector. Specifically, the local density approximation for the semi-infinite jellium model is used to obtain the nonlocal response functions for the *s* electron density. Dynamical screening is treated within a self-consistent field approach. Previous experience has shown that this method yields a nearly quantitative representation of the surface plasmon dispersion of simple metals.[3] The influence of

the *d* electrons is included by representing them in terms of an fcc lattice of point dipoles. The effective atomic polarizability of the *d* shells is chosen to reproduce the measured bulk dielectric function of Ag.[20] The key feature of our combined ''jellium-dipolium'' approach is that the mutual polarization of *s* and *d* electron densities is treated self-consistently without further approximations. We may view this scheme using two equivalent physical pictures: (i) The Ag surface is represented in terms of a semi-infinite, nonlocal homogeneous electron gas whose effective Coulomb interaction is modified as a result of the dipole lattice. (ii) The Ag surface is represented in terms of a semi-infinite lattice of polarizable *d* shells whose dipole interaction is screened via the surrounding nonlocal gas of *s* electrons. An analogous two-component description was used earlier to evaluate the effect of core polarization on the bulk plasma frequency of several metals in the long wavelength limit.[21] The optical response of noble metal clusters has recently also been treated within a similar model.[22]

The macroscopic bulk dielectric function of Ag can be conveniently expressed as[23] $\epsilon(\omega)=\epsilon_s(\omega)+\epsilon_d(\omega)-1$, where $\epsilon_s(\omega)=1-\omega_p^2/\omega(\omega+i\gamma)$ is the Drude function characterizing the *s* electrons and $\epsilon_d(\omega)$ the bound part due to *d* electrons. $\omega_p=9.2$ eV is the bulk plasma frequency corresponding to the *s* electron density and γ a damping parameter. Below the onset of interband transitions at about 3.9 eV, $\epsilon_d(\omega)$ is real, with magnitude ≈ 5.5. Thus, taking into account the screening via *d* bands, the effective bulk and surface plasma frequencies of Ag are $\omega_p^*=\omega_p/\sqrt{\epsilon_d}\approx 3.8$ eV and $\omega_s^*=\omega_p/\sqrt{\epsilon_d+1}\approx 3.7$ eV.

The anomalous blueshift of the Ag surface plasma frequency with increasing $q_\parallel$ can be understood in terms of the spatial variation of the *sd* interaction in the surface region.[17,16] Since the spill out of the electronic density in the vacuum stems primarily from the *s* electrons, the Coulomb interaction due to the outer part of the fluctuating surface plasmon charge is not subject to *sd* screening. Moreover, at finite $q_\parallel$ *sd* screening inside the metal diminishes because of the reduced penetration depth of the dynamical potential. Both mechanisms give rise to a blueshift of the surface plasma frequency. The calculations show that this effect is large enough to offset the usual redshift obtained for simple metals, i.e., the overall dispersion is positive in agreement with experimental observations. An analogous physical mechanism is believed to be responsible for the anomalous blue shift of the Mie resonance of Ag particles with inverse radius.[22,24]

Here we focus on the influence of the crystalline geometry on the dispersion of the Ag surface plasmons. As mentioned above, this effect manifests itself in the different slopes of the dispersion detected for different crystal orientations and, on the (110) face, for orthogonal parallel wave vectors. The latter effect is intimately related to the optical reflectance anisotropy observed on Ag(110).[25,26] In the present approach, lattice effects are associated with the dipole-dipole interactions within atomic planes parallel to the surface and between planes. The geometry and density of dipoles within planes, and the interplanar spacings vary for different crystal orientations. Because of the limited penetration depth of the dynamical potential at finite $q_\parallel$, screening via these dipoles leads to a dependence of the surface plasma frequency on crystal orientation.

The outline of this paper is as follows. In Sec. II, a general discussion of the two-component *sd* electron model for Ag is presented. Section III addresses some details concerning the choice of the local *d* electron polarizability. In Sec. IV the results are discussed and compared with experimental spectra. A summary is given in Sec. V. Atomic units are used unless noted otherwise (1 Hartree $=27.2$ eV, 1 $a_0=0.529$ Å).

II. TWO COMPONENT ELECTRON MODEL

Let us consider a metal subject to a weak perturbating potential $\phi_{ext}(\vec{r},\omega)$. Within a self-consistent field approach, the induced density $n(\vec{r},\omega)$ and the total dynamical potential $\phi(\vec{r},\omega)$ are related via the linear response equations

$$n(\vec{r},\omega)=\int d^3r'\,\chi^0(\vec{r},\vec{r}\,',\omega)\,\phi(\vec{r}\,',\omega), \tag{1}$$

$$\phi(\vec{r},\omega)=\phi_{ext}(\vec{r},\omega)+\int d^3r' K(\vec{r},\vec{r}\,')\,n(\vec{r}\,',\omega), \tag{2}$$

where $\chi^0(\vec{r},\vec{r}\,',\omega)$ is the nonlocal independent particle susceptibility. In the following, we assume that electronic interactions can be treated within the random phase approximation (RPA), i.e., the kernel $K(\vec{r},\vec{r}\,')$ is the bare Coulomb interaction $1/|\vec{r}-\vec{r}\,'|$. In the time dependent extension of the LDA, K also includes an exchange-correlation contribution.[27]

In a two-component valence electron system such as the *sd* electron densitites of the noble metals, one can distinguish two types of interactions: (i) on the one-electron level, there are hybridization effects which modify the orbital energies and wave functions; (ii) in the dynamical response to the external field, there are mutual polarizations which affect the effective potential and the frequency dependence of excitation spectra. Since the frequencies of the Ag collective modes are below the onset of *sd* interband transitions, they lie in a range of weak *sd* hybridization. We therefore neglect the single-particle coupling and focus instead on *sd* polarization effects. Accordingly, we separate the full susceptibility into independent *s* and *d* contributions:

$$\chi^0(\vec{r},\vec{r}\,',\omega)=\chi_s^0(\vec{r},\vec{r}\,',\omega)+\chi_d^0(\vec{r},\vec{r}\,',\omega). \tag{3}$$

The induced density therefore may be written as $n=n_s+n_d$, where

$$n_{s,d}(\vec{r},\omega)=\int d^3r'\,\chi_{s,d}^0(\vec{r},\vec{r}\,',\omega)\,\phi(\vec{r}\,',\omega). \tag{4}$$

For this charge separation the total dynamical potential takes the form $\phi=\phi_{\rm ext}+\phi_s+\phi_d$, where the potentials induced by *s*,*d* electrons are given by

$$\phi_{s,d}(\vec{r},\omega)=\int d^3r'\,K(\vec{r},\vec{r}\,')\,n_{s,d}(\vec{r}\,',\omega). \tag{5}$$

To solve this system of response equations, we now eliminate the induced s electron density n_s and potential ϕ_s and derive modified external and d electron potentials which account for s electron screening. Combining Eqs. (4),(5), we find

$$n_s(\vec{r},\omega)=\int d^3r'\chi_s(\vec{r},\vec{r}\,',\omega)[\phi_{\rm ext}(\vec{r}\,',\omega)+\phi_d(\vec{r}\,',\omega)], \tag{6}$$

where χ_s is the renormalized s electron susceptibility. Omitting momentarily the integration symbols we can express χ_s in terms of χ_s^0 schematically via $\chi_s=\chi_s^0/(1-K\chi_s^0)$. Thus, $\phi_s=Kn_s=K\chi_s(\phi_{\rm ext}+\phi_d)$ and $\phi=(1+K\chi_s)(\phi_{\rm ext}+\phi_d)$. This reformulation of the response equations shows that the total dynamical potential now consists only of external and induced d electron contributions which are, however, screened due to the presence of the nonlocal s electron gas. We point out that this s electron screening involves the renormalized susceptibility χ_s rather than the bare χ_s^0. This ensures that the screening of the external and d electron potentials takes place via a fully interacting s electron gas rather than a gas of independent s electrons.

For completeness we note that elimination of n_d and ϕ_d rather than n_s and ϕ_s from the initial response equations leads to an equivalent expression for the total dynamical potential: $\phi=(1+K\chi_d)(\phi_{\rm ext}+\phi_s)$, where χ_d is the renormalized d electron susceptibility $\chi_d=\chi_d^0/(1-K\chi_d^0)$. In this case, the ϕ consists of external and induced s electron contributions which are screened due to the presence of interacting d electrons.

So far, the reorganization of the response equations is purely formal and depends only on the distinction of s and d contributions to the full susceptibility χ^0 as indicated in Eq. (3). To proceed we now assume that lattice effects on the ground state s electron density are weak so that χ_s^0 can be approximated in terms of the nonlocal response function of a semi-infinite homogeneous electron gas. The local density approximation (LDA) is used for this jellium system[28] to evaluate the wave functions and Green's functions needed for the construction of χ_s^0. We assume furthermore that the d electrons are well localized and that overlap between neighboring sites can be neglected. For simplicity we represent these occupied d shells by dipoles located at the sites of a semi-infinite fcc lattice. The noninteracting d electron susceptibility χ_d^0 can then be approximated as a lattice sum of single-site contributions

$$\chi_d^0(\vec{r},\vec{r}\,',\omega)\approx\sum_i \chi_i^0(\vec{r}-\vec{R}_i,\vec{r}\,'-\vec{R}_i,\omega), \tag{7}$$

where $\vec{R}_i$ denotes a lattice vector. From Eq. (4) it follows that the induced d electron density n_d is also given by a sum over lattice sites, $n_d=\Sigma_i n_i$, where n_i is the d electron density induced at site i.

Let us now place the origin of the coordinate system at site i. The induced d electron density at this site is given by

$$n_i(\vec{r},\omega)=\int d^3r'\,\chi_i^0(\vec{r},\vec{r}\,',\omega)\,\phi(\vec{r}\,',\omega). \tag{8}$$

The total potential $\phi(\vec{r},\omega)$ acting on the d electron shell can be represented in terms of four contributions: the external potential, the potential due to s electrons, the potential due to d electrons at other lattice sites, and the potential induced by the d shell at site i itself. The first three contributions will be referred to as local potential $\phi_{\rm loc}$ and the last one as ϕ_i. Thus, $\phi=\phi_{\rm loc}+\phi_i$. Since the d shells are assumed to be localized, the local potential varies slowly across the site and can be expanded as

$$\phi_{\rm loc}(\vec{r},\omega)\approx\phi_{\rm loc}(\vec{R}_i,\omega)-\vec{r}\cdot\vec{E}_{\rm loc}(\vec{R}_i,\omega)\cdots, \tag{9}$$

where $\vec{E}_{\rm loc}$ is the local electric field at site i. To lowest order, the induced d electron density is therefore determined by the single-site response equation

$$\begin{aligned} n_i(\vec{r},\omega)&=\int d^3r'\,\chi_i^0(\vec{r},\vec{r}\,',\omega)[\phi_i(\vec{r}\,',\omega)-\vec{r}\,'\cdot\vec{E}_{\rm loc}(\vec{R}_i,\omega)] \\ &\equiv c(r,\omega)\,\vec{r}\cdot\vec{E}_{\rm loc}(\vec{R}_i,\omega). \end{aligned} \tag{10}$$

The last identity follows from the assumed spherical symmetry of the d shell and $c(r,\omega)$ specifies the radial dependence of the polarization function. The dipole moment of n_i is $\vec{p}_i(\omega)=\alpha(\omega)\,\vec{E}_{\rm loc}(\vec{R}_i,\omega)$, where the local polarizability is defined as $\alpha(\omega)=\frac{1}{3}\int d^3r\,r^2\,c(r,\omega)$. For simplicity we assume this polarizability to be the same on all lattice sites. In a more refined treatment, this restriction can easily be relaxed. Within the dipole approximation the potential generated by the d electrons is

$$\phi_d(\vec{r},\omega)=-\sum_i \nabla\frac{1}{|\vec{r}-\vec{R}_i|}\cdot\vec{p}_i(\omega). \tag{11}$$

This expression shows that the problem of calculating the d electron contribution to the total potential is reduced to finding the dipole moments $\vec{p}_i(\omega)$. For point like dipoles the above expression for ϕ_d is valid throughout space and the induced d electron density is given by $n_d(\vec{r},\omega)=-\Sigma_i\,\vec{p}_i(\omega)\cdot\nabla\,\delta(\vec{r}-\vec{R}_i)$.

The local field at site i can be written as (for brevity we omit frequency arguments of electric fields and dipole moments)

$$\begin{aligned} \vec{E}_{\rm loc}(\vec{R}_i)&=-\nabla[\phi(\vec{r},\omega)-\phi_i(\vec{r},\omega)]|_{\vec{r}=\vec{R}_i} \\ &=\vec{E}^s_{\rm ext}(\vec{R}_i)+\sum_j \vec{U}^s_{ij}\cdot\vec{p}_j\,. \end{aligned} \tag{12}$$

The first term represents the external field at site i screened via the s electrons

$$\vec{E}^s_{\rm ext}(\vec{R}_i) = -[\nabla \phi^s_{\rm ext}(\vec{r},\omega)]|_{\vec{r}=\vec{R}_i}$$

$$\phi^s_{\rm ext} = (1+K\chi_s)\,\phi_{\rm ext}. \tag{13}$$

Note that the screened external potential $\phi^s_{\rm ext}$ corresponds to the self-consistent local potential of a semi-infinite electron gas in the absence of d electrons. The second term in Eq. (12) accounts for the screened dipole-dipole interaction $\vec{\vec{U}}^s_{ij} = \vec{\vec{U}}_{ij} + \vec{\vec{U}}'_{ij}$. The bare interaction is given by

$$\vec{\vec{U}}_{ij} = \left(\nabla\nabla \frac{1}{|\vec{r}-\vec{R}_j|} \right)|_{\vec{r}=\vec{R}_i}. \tag{14}$$

We use the convention $\vec{\vec{U}}_{ii} \equiv 0$ since the field due to the dipole at site i is subtracted in Eq. (12). The screening via s electrons is described by the tensor (integration symbols are again suppressed):

$$\vec{\vec{U}}'_{ij} = \left(\nabla K\chi_s \nabla \frac{1}{|\vec{r}-\vec{R}_j|} \right)\Bigg|_{\vec{r}=\vec{R}_i}. \tag{15}$$

From the definition of $\vec{p}_i$ we now obtain the following self-consistent equations for the dipole moments

$$\vec{p}_i = \alpha(\omega)\left[\vec{E}^s_{\rm ext}(\vec{R}_i) + \sum_j \vec{\vec{U}}^s_{ij}\cdot\vec{p}_j \right]. \tag{16}$$

Except for the screening of the external field and dipole-dipole interaction, these equations are analogous to those of a pure dipole lattice.

The derivation discussed so far is rather general and applies to arbitrary three-dimensional systems. We now consider explicitly a semi-infinite metal exposed to an external potential whose spatial variation is given by $\phi_{\rm ext}(\vec{r},\omega) = -(2\pi/q)\, e^{i\vec{q}\cdot\vec{r}_\parallel} e^{qz}$, where $\vec{q}$ is a two-dimensional wave vector parallel to the surface and $q = |\vec{q}\,|$. The surface lies in the xy plane and the z axis points towards the vacuum. Because of the translational symmetry parallel to the surface it is convenient to perform a two-dimensional Fourier transform of quantities associated with the s electron component of the system. Since the ground state s electron density is assumed to be homogeneous in the xy plane, the susceptibility $\chi^0_s(\vec{r},\vec{r}\,',\omega)$ depends only on the difference $(\vec{r}_\parallel - \vec{r}\,'_\parallel)$. Thus the Fourier transform may be written as $\chi^0_s(z,z',\vec{q},\omega)$. The screened s electron susceptibility χ_s also has this form since the Coulomb interaction does not modify the symmetry in the surface plane, i.e., we have $\chi_s(z,z',\vec{q},\omega)$. Of course, normal to the surface translational symmetry is broken, so χ^0_s and χ_s are nonlocal functions of z,z'. The dipole lattice introduces periodic modulations in the induced s electron density which are characterized by two-dimensional reciprocal vectors $\vec{g}$. The overall spatial dependence of n_s is therefore of the form

$$n_s(\vec{r},\omega) = \sum_{\vec{g}} e^{i(\vec{q}+\vec{g})\cdot\vec{r}_\parallel} n_s(z,\vec{q}+\vec{g},\omega). \tag{17}$$

The dipole moments within planes parallel to the surface differ only by a phase factor. Let us define a layer index n and express an arbitrary lattice vector as $\vec{R}_i = (\vec{P}+\vec{d}_n, z_n)$, where $\vec{P}$ is a two-dimensional intraplanar lattice vector and $(\vec{d}_n, z_n)$ specifies the origin of the nth plane. Thus, the dipole moment at site i can be represented as $\vec{p}_i = \vec{p}_n\, e^{i\vec{q}\cdot\vec{P}}$. Within this representation, Eq. (16) for the site-dependent dipole moments $\vec{p}_i$ can be reformulated in terms of an equivalent equation for the planar dipole moments $\vec{p}_n$,

$$\vec{p}_n = \alpha(\omega)\left[\vec{E}^s_{\rm ext}(z_n) + \sum_m \vec{\vec{T}}^s_{nm}\cdot\vec{p}_m \right], \tag{18}$$

with $\vec{\vec{T}}^s_{nm} = \vec{\vec{T}}_{nm} + \vec{\vec{T}}'_{nm}$. The tensor describing the unscreened dipole interaction between planes is

$$\vec{\vec{T}}_{nm} = \left(\nabla\nabla {\sum_{\vec{P}}}' \frac{e^{i\vec{q}\cdot\vec{P}}}{|\vec{r}-(\vec{d}_m+\vec{P},z_m)|} \right)\Bigg|_{\vec{r}=(\vec{d}_n,z_n)}, \tag{19}$$

where the prime implies that the term $\vec{P}=0$ must be excluded from the sum in the diagonal element $\vec{\vec{T}}_{nn}$. The evaluation of these tensor elements using the Ewald summation technique[29] was discussed previously.[16]

The tensor $\vec{\vec{T}}'_{nm}$ describing the screening of the dipole interaction between planes via the surrounding s electron density can be derived by a Fourier transformation of Eq. (15). Thus, the two-dimensional transform of the Coulomb kernel is given by $K(z,z',\vec{q}+\vec{g}) = 2\pi\, e^{-|\vec{q}+\vec{g}||z-z'|}/|\vec{q}+\vec{g}|$, and

$$\vec{\vec{T}}'_{nm} = \frac{1}{A}\sum_{\vec{g}} e^{i(\vec{q}+\vec{g})\cdot(\vec{d}_n-\vec{d}_m)} \int dz'\, \vec{L}_{\vec{g}}(z_n,z') \times \int dz''\, \chi_s(z',z'',\vec{q}+\vec{g},\omega)\, \vec{L}_{\vec{g}}(z'',z_m). \tag{20}$$

Here, A is the area of the surface unit cell and $\vec{L}_{\vec{g}}(z,z') = 2\pi[i(\vec{q}+\vec{g}), \partial_z] e^{-|\vec{q}+\vec{g}||z-z'|}/|\vec{q}+\vec{g}|$.

Equation (18) may readily be solved via matrix inversion. Because of the limited penetration depth of the screened external and total dynamical field at finite $\vec{q}$, only a finite number of lattice planes needs to be taken into account. The number of planes depends on the magnitude of $\vec{q}$ and on the interplanar distance for a given crystal orientation. To determine the frequency dependence of the surface excitation spectrum we evaluate first the Fourier components of the d electron potential Eq. (11),

$$\phi_d(z,\vec{q}+\vec{g},\omega) = -\frac{1}{A}\sum_n e^{-i(\vec{q}+\vec{g})\cdot\vec{d}_n}\, \vec{p}_n\cdot\vec{L}_{\vec{g}}(z,z_n). \tag{21}$$

The components of the induced s electron density are then given by

$$n_s(z,\vec{q}+\vec{g},\omega)=\int dz'\,\chi_s(z,z',\vec{q}+\vec{g},\omega)\times[\phi_{\rm ext}(z',\vec{q}+\vec{g},\omega)+\phi_d(z',\vec{q}+\vec{g},\omega)]. \tag{22}$$

The surface response function $g(\vec{q},\omega)$ can be obtained from the asymptotic behavior of the $\vec{g}=0$ component of the induced *s* and *d* electron potentials far in the vacuum[30] $\phi_s+\phi_d\rightarrow(2\pi/q)\,e^{-qz}\,g(\vec{q},\omega)$ for $z\gg 0$. Thus,

$$g(\vec{q},\omega)=\int dz\,e^{qz}\,n_s(z,\vec{q},\omega)-\frac{1}{A}\sum_n e^{-i\vec{q}\cdot\vec{d}_n}\,e^{qz_n}\,\vec{p}_n\cdot[i\vec{q},-q]\equiv g_s(\vec{q},\omega)+g_d(\vec{q},\omega). \tag{23}$$

The imaginary part of this quantity provides the surface loss function which can be compared with energy loss spectra obtained in inelastic electron scattering measurements. The position of the maxima of Im $g(\vec{q},\omega)$ plotted as a function of ω for a given $\vec{q}$ will be used to determine the resonance frequency $\omega_s(\vec{q})$ of the collective surface excitation for a given crystal orientation.

We close this section by pointing out that the computational effort to evaluate the surface excitation spectra within the ''jellium-dipolium'' model is not significantly greater than for the individual models. The matrix equation for the induced dipole moments p_n has about the same dimension as in the pure dipolium case and the incorporation of *s* electron screening requires evaluation of χ_s^0 and inversion of $(1-K\chi_s^0)$. The main new task is that $\chi_s^0(z,z',\vec{q}+\vec{g},\omega)$ must be calculated for all $|\vec{q}+\vec{g}|$ rather than only $\vec{g}=0$ as for bare jellium.

III. LOCAL POLARIZABILITY

The key quantity determining the influence of the *d* electrons on the surface loss function derived above is the local polarizability $\alpha(\omega)$. In principle, this function could be calculated self-consistently using the single-site response equation (10). The solution of Eq. (16) for a three-dimensional bulk system then yields a relationship between the total potential $\phi(\vec{r},\omega)$ and the applied external potential $\phi_{\rm ext}(\vec{r},\omega)$. Fourier transforming these quantities and taking the long wavelength limit $\vec{q}\rightarrow 0$ gives the macroscopic dielectric function of the system. This procedure was used previously[21] to determine the effect of core polarization on the dielectric response of simple metals. Since our main interest here is not the bulk but the surface, we instead choose $\alpha(\omega)$ to reproduce the measured bulk dielectric function $\epsilon(\omega)$.[20] In the bulk $\alpha(\omega)$ is given by the modified Clausius-Mossotti (CM) relation[21]

$$\frac{4\pi}{3}n\alpha=\frac{(\epsilon-\epsilon_s)}{3+(\epsilon-\epsilon_s)(1+\Sigma)}, \tag{24}$$

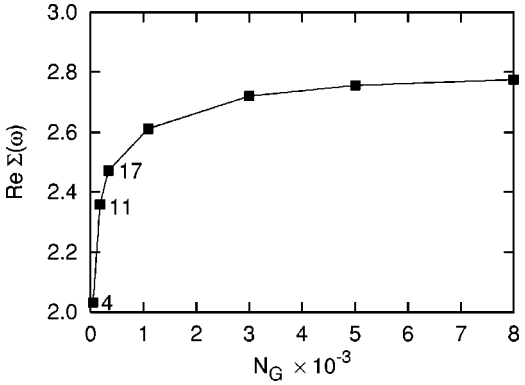

FIG. 1. Re $\Sigma(\omega)$ as a function of the number N_G of bulk reciprocal vectors. The Lindhard dielectric function is evaluated for an electron gas with $r_s=2.97\ a_0$ at $\omega=3.6$ eV. The numbers denote the closed shells of $\vec{G}$ corresponding to some N_G.

where *n* is the atomic density, $\epsilon_s(\omega)$ the *s* electron Drude dielectric function, and the coefficient

$$\Sigma(\omega)=\sum_{\vec{G}\neq 0} f(\vec{G},\omega)\,[1-1/\epsilon_L(\vec{G},\omega)] \tag{25}$$

accounts for *s* electron density fluctuations induced by the short-wavelength local fields due to the *d* shells. $\epsilon_L(\vec{G},\omega)$ is the Lindhard dielectric function at the bulk reciprocal lattice vector $\vec{G}$. In the case of point dipoles, $f(\vec{G},\omega)=1$ for all $\vec{G}$ while, for dipoles of finite size, the magnitude of *f* diminishes rapidly with growing $\vec{G}$.[21] Neglecting the local fields induced in the *s* electron density, i.e., $\Sigma(\omega)=0$, one recovers the usual CM expression for the polarizability.

The derivation of the surface loss function discussed in the previous section is based on the assumption of point dipoles. The quantity affected by this assumption is the screening part of the dipole-dipole interaction defined in Eqs. (15) and (20). Since for computational reasons only a finite number of surface reciprocal lattice vectors $\vec{g}$ can be considered in the expansion of $\overleftrightarrow{T}'$, truncation errors are unavoidable. To estimate the influence of such a truncation in the case of the bulk, it is instructive to study the convergence of the coefficient $\Sigma(\omega)$ with the number N_G of vectors $\vec{G}$ included in the sum in Eq. (25). This is illustrated in Fig. 1 which shows Re $\Sigma(\omega)$ as a function of N_G for a frequency in the range of interest for Ag surface plasmons.

The slow convergence of $\Sigma(\omega)$ is a consequence of the highly localized screening charge induced by the singular point dipole potential. As mentioned above, taking into account the finite size of the dipoles leads to a significantly more rapid convergence as a function of $\vec{G}$.[21] On the other hand, truncating the sum in Eq. (25) after a few shells leads to a reduction of Re $\Sigma(\omega)$ of the order of 20 to 30 %. Thus, in order to reproduce the measured dielectric function, the local polarizability must be adjusted. Figure 2 shows the frequency dependence of $\alpha(\omega)$ near the interband onset for several values of Re Σ. (Since the frequency variation of Σ in the range of interest is negligible compared to the truncation effects, we omit it in the following.) The reduction of

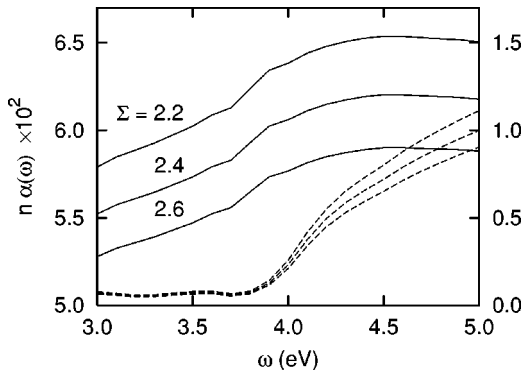

FIG. 2. Atomic d electron polarizability $\alpha(\omega)$ per unit volume for different values of Re Σ ($n=0.058$ Å^{-3}). Solid curves: real part (left scale), dashed curves: imaginary part (right scale).

Re Σ due to truncation of the sum over $\vec{G}$ is seen to give an enhancement of Re $\alpha(\omega)$ of the order of 10%. Since a larger d shell polarizability implies stronger sd screening, the frequency of the surface plasma oscillation is lowered. In the case of the Ag low-index crystal faces, the different intraplanar geometries and interplanar spacings give rise to slightly different frequency shifts if a finite number of surface reciprocal lattice vectors is retained in the calculation of surface loss spectra. One must therefore be careful when comparing excitation frequencies for different crystal faces. This problem will be addressed in more detail in the next section.

We briefly point out here that the present definition of $\alpha(\omega)$ cannot be used if the screening of dipole interactions is treated using a local s electron gas. In this case the interaction of a dipole with the charge induced by its own field diverges. To exclude this screened self-interaction a different definition of the polarizability in terms of the remaining screened field must be found. The relation between $\alpha(\omega)$ and the macroscopic dielectric function is in this case given by

$$\frac{4\pi}{3} n\alpha = \frac{\epsilon_s(\epsilon-\epsilon_s)}{3\epsilon_s+(\epsilon-\epsilon_s)} \tag{26}$$

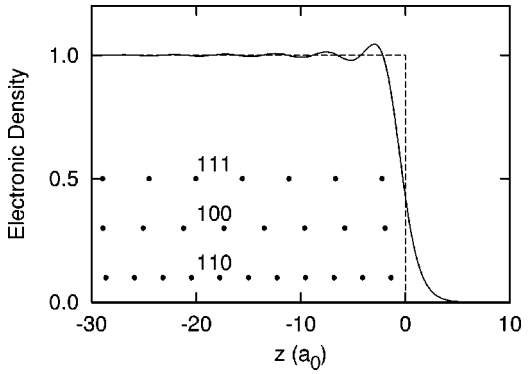

FIG. 3. Schematic representation of Ag two component sd electron model. The ground state s electron density (normalized to n_b; solid curve) is calculated within the LDA for a semi-infinite jellium system. The positive background (dashed line) occupies the half-space $z \leqslant 0$. The symbols mark the positions of the lattice planes for the three low-index faces of the fcc crystal. The $4d$ shells at the lattice sites are represented via point dipoles.

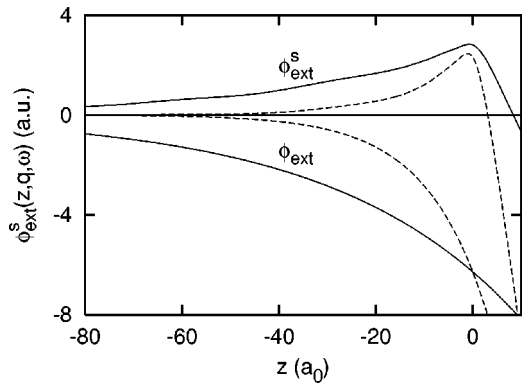

FIG. 4. Comparison of real part of screened external potential $\phi^s_{\rm ext}(z,\vec{q},\omega)$ in the absence of d electrons with bare external potential $\phi_{\rm ext}(z,\vec{q},\omega)$ for $\omega=3.6$ eV. Solid curves: $q=0.05$ Å^{-1}, dashed curves: $q=0.15$ Å^{-1}.

which is also consistent with the CM formula. A comparison between the polarizability obtained for a local screening model and the present nonlocal Lindhard screening is not meaningful since an important physical difference exists between the definitions of the screened fields in these two models.

IV. RESULTS AND DISCUSSION

A schematic representation of the two-component sd electron model is given in Fig. 3. The ground state density profile is obtained using the LDA for a semi-infinite electron gas of density $n_b=3/(4\pi r_s^3)$ with $r_s=2.97$ a_0 yielding the Ag Drude plasma frequency 9.2 eV. The dipoles occupy the sites of a semi-infinite fcc lattice with room temperature lattice constant $a=4.09$ Å . The symbols indicate the positions of the atomic planes for the three low-index faces. The first plane is half a lattice spacing away from the jellium edge and the interplanar distances are $0.5a$, $a/\sqrt{3}$, and $a/(2\sqrt{2})$ for the (100), (111), and (110) faces, respectively. The response

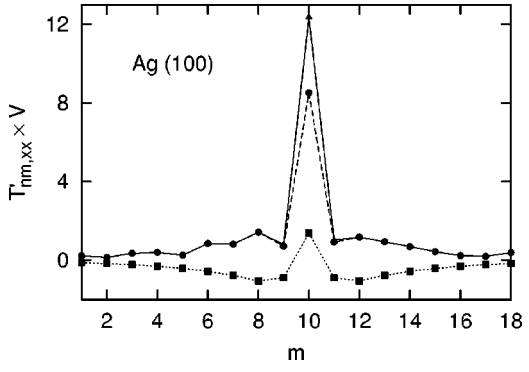

FIG. 5. Real part of xx component of screening contribution $\vec{\vec{T}}'_{nm}(\vec{q},\omega)$ to dipole interaction tensor as a function of layer index m for fixed $n=10$. The tensor elements are multiplied by the atomic volume of Ag [$\omega=3.7$ eV, $q=0.15$ Å^{-1}, (100) face]. Solid curve: $N_g=21$; dashed curve: $N_g=5$, where N_g represents the number of surface reciprocal vectors included in the screening calculation. Dotted curve: xx component of unscreened tensor $\vec{\vec{T}}_{nm}(\vec{q})$.

calculations are carried out at complex frequencies, with the imaginary component accounting for the Drude damping derived from the measured bulk dielectric function.

According to Eq. (18), the effective electric field driving the dipoles is determined by the screened external potential $\phi^s_{\rm ext}(z,\vec{q},\omega)$ which corresponds to the self-consistent potential in the absence of *d* electrons. Figure 4 illustrates this potential for typical wave vectors $\vec{q}$. The comparison with the bare external potential $\phi_{\rm ext}\sim e^{qz}$ shows that although the screened potential has a much smaller amplitude within the metal, its tail also decays as $\sim e^{qz}$ towards the interior. This penetration depth determines the number of dipole planes for a given crystal face that need to be taken into account to achieve convergence. In the limit of small $\vec{q}$ this depth becomes very large, indicating that polarization of the entire half-space contributes to the dielectric response of the surface.

The key quantity specifying the variation of surface excitation spectra with crystal structure in the present model is the screened dipole interaction tensor $\vec{\vec{T}}^s_{nm}(\vec{q},\omega)$. Of particular interest is the competition between the bare or direct interaction $\vec{\vec{T}}_{nm}(\vec{q})$ and the indirect contribution $\vec{\vec{T}}'_{nm}(\vec{q},\omega)$ mediated via the *s* electron density [see Eqs. (19) and (20)]. Figure 5 shows the *xx* components of $\vec{\vec{T}}_{nm}$ and $\vec{\vec{T}}'_{nm}$ as a function of *m* for a fixed *n*. The magnitude of both elements decays to zero as $|n-m|$ increases, implying a limited range of interaction between neighboring planes. This is the general behavior of all tensor components at finite values of $\vec{q}$. The screening element $\vec{\vec{T}}^s_{nm}$ depends on ω. However, in the narrow frequency range of interest for Ag surface plasmons this variation is very slight.

The direct and indirect interplanar contributions to $\vec{\vec{T}}^s_{nm}$ are seen be of similar magnitude with opposite signs. This tendency is quite general, indicating a significant overall change of interactions between *d* shells as a result of the surrounding gas of *s* electrons. The intraplanar tensor elements cannot be compared directly since the self-interaction is excluded from the bare interaction while it is present in the indirect screening element. For this reason, $\vec{\vec{T}}'_{nn}$ can be much larger than $\vec{\vec{T}}_{nn}$.

The interaction tensors have a complicated dependence on wave vector. In general increasing *q* leads to a shorter interaction range and to decaying tensor elements for planes n,m which are far apart. On the other hand, the interaction between closely spaced planes can be enhanced for increasing *q* since it depends also on the relative lateral position of the dipoles. Moreover, these effects vary with crystal orientation because of the different intraplanar and interplanar geometries.

For $n\neq m$ the screened tensor $\vec{\vec{T}}'_{nm}$ involves indirect interactions between dipoles and the charges induced in other planes. As shown Fig. 5, the sum over reciprocal vectors $\vec{g}$ in Eq. (20) converges after a few terms because of the rapidly decaying Coulomb field. On the other hand, for $n=m$ the tensor element includes the interaction of a dipole with the charge induced at the same site. The Fourier representation of this localized charge requires many $\vec{g}$. Accordingly, the sum over $\vec{g}$ converges more slowly than for $n\neq m$ (see Fig. 5). Evidently, the contributions to $\vec{\vec{T}}'_{nn}$ due to large $\vec{g}$ are generated primarily by this self-interaction. They carry no information about neighboring sites within the same plane. A similar effect was discussed in the previous section when addressing the local polarizability in the bulk case.

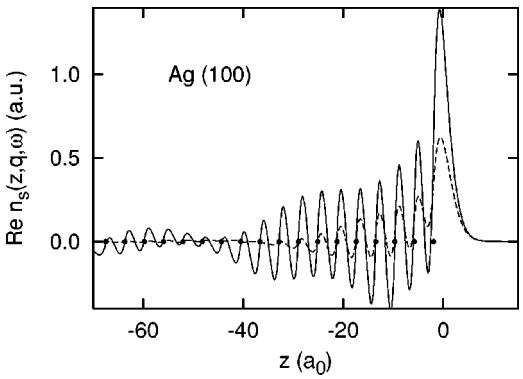

FIG. 6. Real part of $\vec{g}=0$ component of induced *s* electron density $n_s(z,\vec{q},\omega)$ for Ag(100), $\omega=3.67$ eV. Solid curve: $q=0.1$ Å^{-1}, dashed curve: $q=0.2$ Å^{-1}. The dots indicate the positions of the lattice planes.

For computational reasons it is necessary to limit the calculation of $\vec{\vec{T}}'_{nm}$ to a finite set of reciprocal vectors $\vec{g}$. As pointed out above, this amounts to an approximation of the self-field of each dipole. In order to keep the surface response calculation consistent with the bulk model used for the definition of $\alpha(\omega)$, it is therefore important to exclude in the bulk case the corresponding terms associated with the screening contribution due to the dipolar self-field. Thus, in Eq. (25) the large $\vec{G}$ terms should be omitted. However, terms arising in the three-dimensional $\vec{G}$ representation cannot be directly compared with the two-dimensional surface analog. It is possible to express Σ defined by Eq. (25) using a two-dimensional representation of the dipole interaction

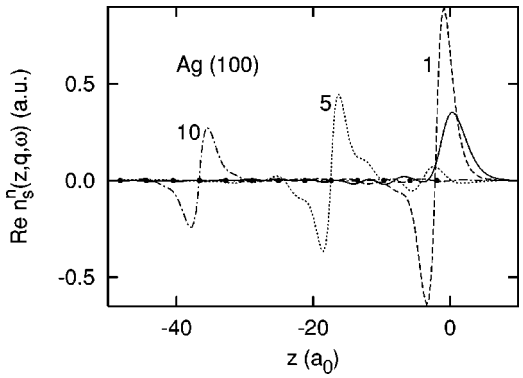

FIG. 7. Contributions to induced *s* electron density shown in Fig. 6 for $q=0.1$ Å^{-1}. Solid curve: Re $n_0(z,\vec{q},\omega)$ induced by external field; dashed, dotted, dash-dotted curves: Re $n^n_s(z,\vec{q},\omega)$ induced by dipole planes $n=1$, 5, 10, respectively. The dots indicate the positions of the dipole planes.

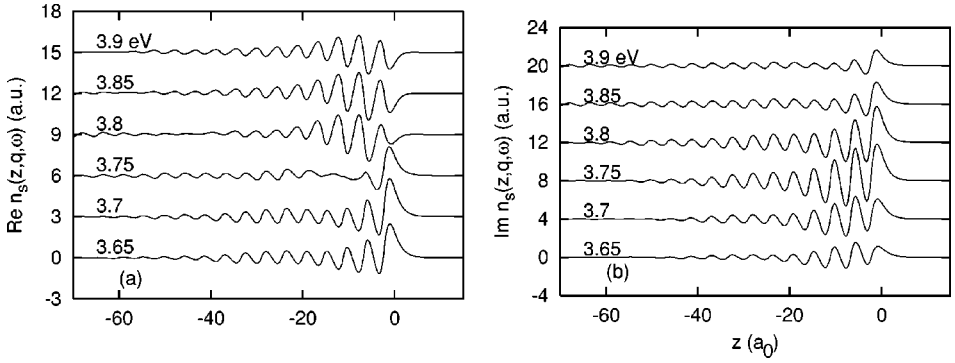

FIG. 8. Induced s electron density $n_s(z,\vec{q},\omega)$ for Ag(111), $\vec{q}=0.1$ Å^{-1}. (a) Real part; (b) imaginary part. The frequency varies between $\omega=3.65$ and 3.9 eV. The curves are vertically displaced for clarity.

$$\Sigma(\omega)=\frac{3}{4\pi}\lim_{n\to\infty}\lim_{q\to 0}\sum_{m}[\vec{\vec{T}}'_{nm}(\vec{q},\omega)]_{xx}. \tag{27}$$

Unfortunately, the definition of $\vec{\vec{T}}'_{nm}$ given in Eq. (20) cannot be used in the limit $q\to 0$ because of the diverging range of the Coulomb interaction. Qualitatively, however, it is clear that truncation of the sum over $\vec{g}$ in this definition is related to a truncation of the sum over $\vec{G}$ in the definition of Σ, Eq. (25). As illustrated in Figs. 1 and 2, this implies a reduction of the magnitude of Σ and an enhancement of $\alpha(\omega)$. In principle, the truncation could affect the parallel and perpendicular tensor components in a different manner, resulting in different enhancements of $\alpha(\omega)_{\parallel}$ and $\alpha(\omega)_{\perp}$. In the calculations discussed below, we ignore such anisotropy effects. However, to estimate the overall influence of the truncation of the $\vec{g}$ sum in Eq. (20), we present results for typical values of Σ. Fortunately, the uncertainty implied by this truncation is reduced appreciably by the requirement that in the $q\to 0$ limit all three low-index faces must yield the same surface plasma frequency.

The induced s electron density $n_s(\vec{r},\omega)$ defined in Eq. (17) exhibits spatial fluctuations due to various wave vector contributions. The most relevant component is the $\vec{g}=0$ term which is used to calculate the surface response functions, Eq. (23). Because of the form of the external potential the first term in Eq. (22) is finite only for $\vec{g}=0$. This induced density is therefore the same as for pure jellium in the absence of d electrons. We denote this contribution as $n_0(z,\vec{q},\omega)$. Because of the form of the d electron potential defined in Eq. (21), the second term in Eq. (22) induced by the dipoles can be expressed as a sum over lattice planes. Thus, we may write the $\vec{g}=0$ contribution as $n_s=n_0+\Sigma_n n_s^n$. This induced density is shown in Fig. 6 for two values of $\vec{q}$. With increasing $\vec{q}$ the density decays more rapidly because of the shorter penetration depth of the perturbating potential. Superimposed on the oscillations due the dipole planes are Friedel oscillations caused by the Fermi cut off in the sum over occupied states in the susceptibility $\chi_s(z,z',\vec{q}+\vec{g},\omega)$.

To analyze the density oscillations induced by the d electrons, we show in Fig. 7 the contribution to $n_s(z,\vec{q},\omega)$ due to the external potential and due to several dipole planes. Apart from weak Friedel oscillations, $n_0(z,\vec{q},\omega)$ is localized in the region close to the surface. Although the contribution from a given dipole plane is localized near that plane (note, however, the Friedel oscillations due to the fifth plane extending all the way to the surface), even rather deep planes produce significant induced densities so that the overall penetration depth of the total $n_s(z,\vec{q},\omega)$ is very much larger than that of $n_0(z,\vec{q},\omega)$ for the bare jellium surface.

Figure 8 shows the induced s electron density $n_s(z,\vec{q},\omega)$ for Ag(111) at several frequencies. The resonance frequency 3.75 eV is characterized by the sign change of Re n_s and the

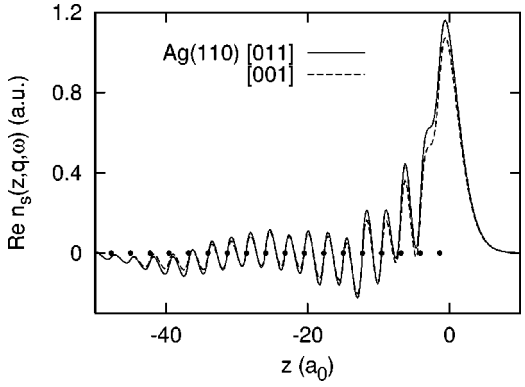

FIG. 9. Real part of induced s electron density $n_s(z,\vec{q},\omega)$ for Ag(110)[001] (dashed curve) and Ag(110)[011] (solid curve). $\vec{q}=0.1$ Å^{-1}, $\omega=3.67$ eV. The dots indicate the positions of the dipole planes.

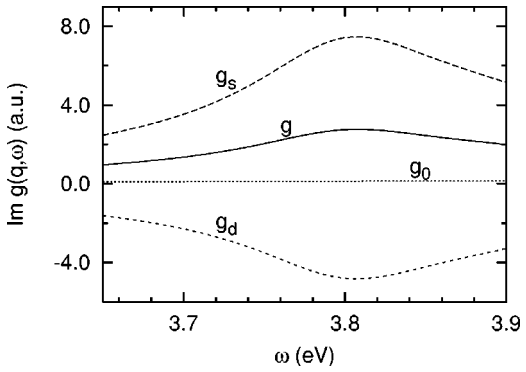

FIG. 10. Surface excitation spectrum for Ag(100). Solid curve: full spectrum Im $g(\vec{q},\omega)$; dashed and dotted curves: s and d electron contributions Im $g_{s,d}(\vec{q},\omega)$; dash-dotted curve: bare jellium loss function Im $g_0(\vec{q},\omega)$. $\vec{q}=0.1$ Å^{-1}, $\Sigma=2.35$.

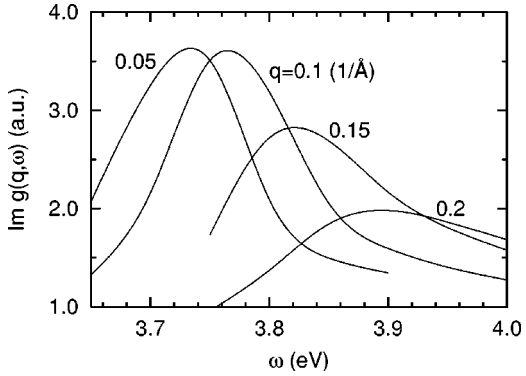

FIG. 11. Surface loss spectra Im $g(\vec{q},\omega)$ for Ag(111) for several parallel wave vectors. $\Sigma=2.35$.

increase in magnitude of Im n_s. Again, only the $\vec{g}=0$ Fourier component is plotted. As discussed above, the spatial oscillations originate from the dipoles located at the atomic planes and from the frequency dependent Friedel oscillations. Note also that the frequency range shown is just below the range of propagating bulk plasmons since the $\vec{q}=0$ value of the screened volume plasma frequency of Ag is about 3.8 eV. This explains the large penetration depth of the induced charge density at higher frequencies.

The local field at a given site is sensitive to variations in both magnitude and direction of the wave vector. On Ag(110) this leads to an anisotropy of the dipole moments and the induced *s* electron density for orthogonal $\vec{q}$. Figure 9 illustrates this effect for the density n_s. Although the effect of orthogonal $\vec{q}$ on the *sd* screening interaction are difficult to trace in detail, it appears that the lower atomic density in the [001] direction implies a weaker dipole polarization. This mechanism reduces the *sd* screening and gives rise to a higher surface plasma frequency than for the [011] direction. This trend is found also for other values of *q*.

The surface loss function Im $g(\vec{q},\omega)$ can be separated into *s* and *d* electron contributions as indicated in Eq. (23). The local electric field polarizing the *d* shells yields an overall *d* electron polarization with opposite sign. Accordingly, as illustrated in Fig. 10, there is a significant cancellation of *s* and *d* contributions to the loss function. Nevertheless, the frequency variation is nearly the same for both terms since the surface plasmon is a collective excitation of the combined *sd* electron system. In fact, the bare jellium contribution $g_0(\vec{q},\omega)$ corresponding to $n_0(z,\vec{q},\omega)$ is very small and nearly independent of ω. (It's maximum occurs at about 6.5 eV.) Thus, the *s* electron contribution induced by the dipole field ϕ_d is governed by the frequency dependence of the induced dipoles $p_n(\vec{q},\omega)$. The same cancellation of *s* and *d* contributions to the net surface polarization was found previously in the polarizable background model.[18]

Figure 11 shows the surface loss function for Ag(111) for several wave vectors. With increasing $\vec{q}$ the resonance associated with the surface plasmon is seen to shift to higher frequency. The width of the resonance also increases, in particular, on the high-energy side due to the onset of interband transitions near 3.9 eV. Part of the width is due to bulk damping obtained from the Drude contribution of the measured dielectric function. The value of Σ is chosen such that the surface plasma frequency extrapolates in the long wavelength limit to the value measured optically. The response equations in the present model can be solved for $q \geqslant 0.05$ Å^{-1}. At smaller values, convergence becomes difficult because of the rapidly increasing penetration depth of the induced potential. Although there is some uncertainty with respect to the precise form of the dispersion curve at small $\vec{q}$,[18] the resonance maxima in Fig. 11 extrapolate in the $\vec{q}\to 0$ limit to about 3.7 eV in agreement with experiment.

To illustrate the sensitivity of the Ag excitation spectra to the *d* electron polarizability $\alpha(\omega)$ we show in Fig. 12 the dispersion of the surface plasma frequency of Ag(111) and Ag(100) for several values of Σ. As discussed in the previous section, for computational reasons the surface response calculation requires a truncation of the sum over lateral reciprocal lattice vectors $\vec{g}$. Since this amounts to an approximate treatment of the induced dipolar self-field, a consistent bulk description of this field requires an analogous truncation of the sum over bulk reciprocal lattice vectors $\vec{G}$ involved in the local *d* shell polarizability defined in Eqs. (24),(25). As can be seen, a reduction of Σ, i.e., a larger value of $\alpha(\omega)$ implies a lowering of the excitation frequency due to effectively larger *sd* screening. In addition, the dispersion with $\vec{q}$ becomes slightly steeper since the reduced penetration depth of the dynamical potential at larger $\vec{q}$ amounts to a more rapid reduction of *sd* screening and a stronger blue shift of the plasma frequency.

The comparison of the surface plasmon dispersions for Ag(100) and Ag(111) indicates a slightly larger positive slope for the (100) face than for Ag(111) in agreement with

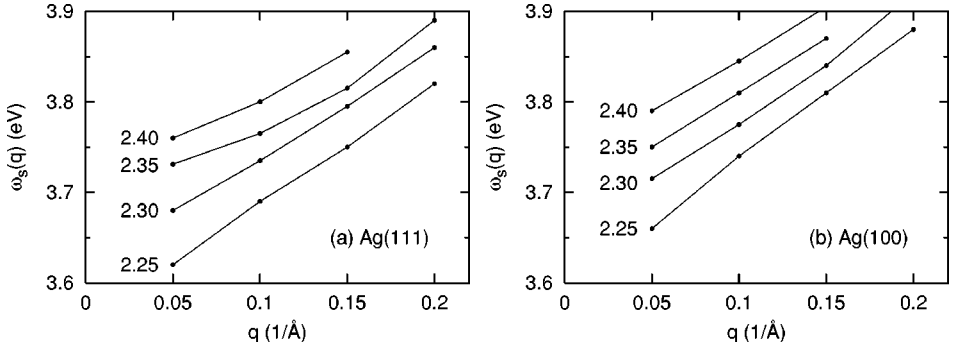

FIG. 12. Surface plasmon dispersion $\omega_s(q)$ for (a) Ag(111) and (b) Ag(100) for several values of Σ. A reduced Σ implies a larger *d* electron polarizability and stronger *sd* screening, giving rise to lower surface plasmon frequencies and a steeper dispersion with $\vec{q}$.

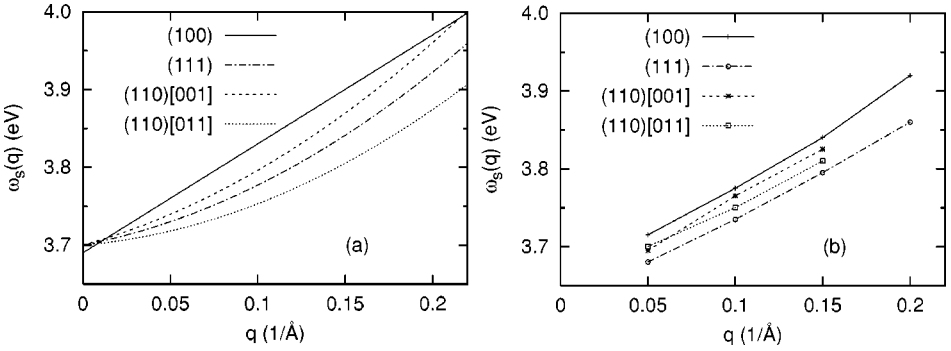

FIG. 13. Surface plasmon dispersion $\omega_s(q)$ for low-index faces of Ag. (a) Experimental data (Refs. 5–7); (b) Calculated dispersions for $\Sigma=2.3$.

experimental observations (see below). The frequency differences are, however, rather small and comparable to the changes introduced by the adjustment of $\alpha(\omega)$ due to the truncation of the reciprocal lattice sums. To ensure that terms of similar size are included for all low-index faces we have truncated the sums over $\vec{g}$ at similar absolute values $|\vec{g}|$. The number of $\vec{g}$ terms therefore depends on the crystal face. Specifically, we have used 21, 19, and 31 surface reciprocal vectors on the (100), (111), and (110) faces, respectively. To compensate for the omitted part of self-field the polarizability $\alpha(\omega)$ is renormalized by reducing the parameter Σ as discussed above.

In Fig. 13 the calculated surface plasmon dispersions for the Ag low-index faces are compared to the experimental results.[5–7] We choose $\Sigma=2.3$ for all faces in order to approximately reproduce the range of observed frequencies. As can be seen, the trend obtained for the different crystal orientations is consistent with the data: (i) the dispersion for Ag(100) lies above that of the (111) face and (ii) the slope for Ag(110)[001] is larger than for Ag(110)[110]. On Ag(110) the long wavelength limit of the surface plasma frequency is the same for both propagation directions regardless of the value of Σ. The dispersions for the two propagation directions illustrate the effect of the intraplanar geometry on the effective local fields. Except, of course, for the lattice effects, the dispersions obtained within the present jellium-dipolium model agree well with those of the isotropic model employing a semi-infinite polarizable medium.[17]

The main difference with respect to the data is that the overall variation of the positive slope with crystal orientation is smaller than found experimentally. Taking into account the finite size of the dipoles representing the *d* electrons presumably leads to even weaker lattice effects because of the smoother spatial variation of the induced *d* electron potential. Thus, part of the observed dependence of the Ag surface plasmon dispersion on crystal structure appears to be associated with the true *s* and *d* electron band structure not captured in the present jellium-dipolium approach.

In view of the small differences between the calculated dispersions we have investigated in more detail the influence of the value of Σ. For the purpose of comparing the dispersions for Ag(100) and Ag(111) let us approximate the results shown in Fig. 12 by linear fits of the form $\omega_s(\vec{q})=aq+b$, where the constants depend on Σ. Figure 14 shows the relationship between the slope *a* and intercept *b* for various values of Σ. Assuming the linear dispersion to be valid down to the $\vec{q}\to 0$ limit, the dispersions for both crystal faces are consistent if they yield the same $\vec{q}=0$ surface plasma frequency. Thus slopes *a* for identical values of *b* should be compared. Although the absolute frequencies for the two faces then become more similar than the ones shown in Fig. 13, the results plotted in Fig. 14 demonstrate that regardless of the choice of Σ, the slope on Ag(100) is about 20% larger than on Ag(111). This suggests that despite the truncation errors introduced in the solution of the response equations, we can be sure that the present model is able to make reliable predictions concerning the face dependence of the Ag surface plasmon dispersion. We note, however, that the assumption of a linear extrapolation of the dispersions to the long wavelength limit might not be accurate.[18] In fact, because of quadratic terms, the true $\vec{q}=0$ frequency is most likely somewhat higher than the intercept *b* shown in Fig. 14. Thus, the linear fit exaggerates the difference between the long wavelength limits for the two faces.

The response calculations discussed above were carried out within the RPA. In the case of simple metals, exchange-correlation contributions to the dynamical potential weaken the bare Coulomb interaction between conduction electrons, giving rise to a slight lowering of the surface plasma frequency at finite $\vec{q}$.[3] A similar redshift was found in the two-component *sd* electron model where the *d* bands were represented in terms of a semi-infinite polarizable medium.[18] In the present jellium-dipolium system, this frequency lowering

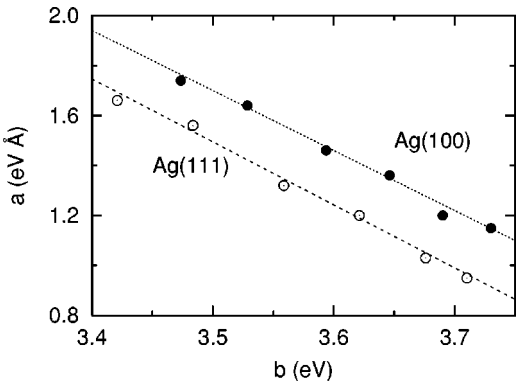

FIG. 14. Parameters *a* and *b* obtained from a linear approximation of the surface plasmon dispersion, $\omega_s(q)=aq+b$ for different values of Σ. Filled dots: Ag(100); empty dots: Ag(111). For each face, the symbols correspond to (from top) $\Sigma=2.15,2.20,\ldots,2.4$.

could, in principle, depend on the crystal face. In view of the overall smallness of this effect, however, we expect the sequence of positive slopes of the dispersions for the Ag low index faces to be unaffected by exchange-correlation contributions.

V. CONCLUSION

A model for the dynamical surface response of the Ag $5s,4d$ valence electrons has been developed in which the mutual polarization of these densities is treated self-consistently. Since the consideration of the full band structure is not yet feasible, the delocalized *s* electron density is treated within the semi-infinite jellium model using the local density approximation and the more localized *d* electrons are represented by a semi-infinite fcc lattice of point dipoles. This combined ''jellium-dipolium'' improves previous schemes which focus on either *s* or *d* electron component but treat the other component more approximately. In particular, both the nonlocal dynamical surface response of the *s* electrons and the crystalline geometry associated with the *d* electrons are taken into account. In addition, the response to finite lateral wave vectors is treated in a nonperturbative manner. Thus, the full range of momenta studied in electron energy loss measurements in accessible.

We have applied our scheme to evaluate energy loss spectra for the low-index faces of Ag with the aim of understanding the dependence of the surface plasmon dispersion relation on crystal orientation. The dispersion with wave vector is positive on all three low-index faces, and the magnitude of the slope varies in a characteristic manner with crystal orientation and propagation direction. These observations are in agreement with experiment. The main difference is that the overall variation of the theoretical dispersions with crystal orientation is smaller than observed in the data. Since the Ag surface collective modes lie just below the onset of interband transitions, this discrepancy might be related to genuine band structure effects ignored in the present approach. The question concerning the large optical anisotropy spectra that has been obtained experimentally for the Ag(110) face also arises. It would be interesting to see if the present model yields a large enough anisotropy for the surface plasmon-polariton propagation in the $q=0$ limit for the different propagation directions on this face.

In future work it would be desirable to allow for the finite extent of the *d* electron densities induced at the lattice sites. This improvement of the point dipole model would eliminate inaccuracies in the present scheme originating from the approximate treatment of the rapidly varying induced dipolar self-field. In addition, it would be interesting to consider a *d* shell polarizability in the surface region that differs from the bulk value. Also, a more realistic description of the *s* electron response could be achieved by incorporating a one-dimensional pseudopotential in the direction normal to the surface.

ACKNOWLEDGMENTS

C.L.B. and W.L.M. acknowledge partial support from DGAPA-UNAM through Grant No. IN-107796 and from the Deutscher Akademischer Austauschdienst DAAD (C.L.B.).

[1] H. Raether, *Surface Plasmons* (Springer, Berlin, 1988).
[2] P. J. Feibelman, Phys. Solid State **12**, 287 (1982).
[3] A. Liebsch, *Electronic Excitations at Metal Surfaces* (Plenum, New York, 1997).
[4] B. Rothenhäusler and W. Knoll, Nature (London) **332**, 615 (1988); G. Flätgen *et al.*, Science **269**, 668 (1998); C. A. Keller, K. Glasmäster, V. P. Zhdanov, and B. Kasemo, Phys. Rev. Lett. **84**, 5443 (2000).
[5] R. Contini and J. M. Layet, Solid State Commun. **11**, 1295 (1972).
[6] S. Suto, K. Tsuei, E. W. Plummer, and E. Burstein, Phys. Rev. Lett. **63**, 2590 (1989); G. Lee, P. T. Sprunger, E. W. Plummer, and S. Suto, *ibid.* **67**, 3198 (1991); Surf. Sci. **286**, L547 (1993).
[7] M. Rocca and U. Valbusa, Phys. Rev. Lett. **64**, 2398 (1990); M. Rocca, M. Lazzarino, and U. Valbusa, *ibid.* **67**, 3197 (1991); **69**, 2122 (1992); M. Rocca, Surf. Sci. Rep. **22**, 1 (1995); F. Moresco, M. Rocca, V. Zielasek, T. Hildebrandt, and M. Henzler, Surf. Sci. **388**, 1 (1997); **388**, 24 (1997).
[8] K. D. Tsuei, E. W. Plummer, and P. J. Feibelman, Phys. Rev. Lett. **63**, 2256 (1989).
[9] K. D. Tsuei, E. W. Plummer, A. Liebsch, K. Kempa, and P. Bakshi, Phys. Rev. Lett. **64**, 44 (1990); K. D. Tsuei, E. W. Plummer, A. Liebsch, E. Pehlke, K. Kempa, and P. Bakshi, Surf. Sci. **247**, 302 (1991).
[10] P. T. Sprunger, G. M. Watson, and E. W. Plummer, Surf. Sci. **269/270**, 551 (1992).
[11] H. Ishida and A. Liebsch, Phys. Rev. B **54**, 14 127 (1996).
[12] R. H. Ritchie, Phys. Rev. **106**, 874 (1957).
[13] M. A. Cazalilla, J. S. Dolado, A. Rubio, and P. Echenique, Phys. Rev. B **61**, 8033 (2000).
[14] P. Monachesi (unpublished).
[15] J. Tarriba and W. L. Mochán, Phys. Rev. B **46**, 12 902 (1992).
[16] C. López-Bastidas and W. L. Mochán, Phys. Rev. B **60**, 8348 (1999).
[17] A. Liebsch, Phys. Rev. Lett. **71**, 145 (1993); Phys. Rev. B **48**, 11 317 (1993).
[18] A. Liebsch and W. L. Schaich, Phys. Rev. B **52**, 14 219 (1995).
[19] P. J. Feibelman, Surf. Sci. **282**, 129 (1993).
[20] P. Johnson and R. W. Christy, Phys. Rev. B **6**, 4370 (1972).
[21] K. Sturm, Solid State Commun. **48**, 29 (1983); K. Sturm, E. Zaremba, and K. Nuroh, Phys. Rev. B **42**, 6973 (1990).
[22] L. Serra and A. Rubio, Phys. Rev. Lett. **78**, 1428 (1997).
[23] H. Ehrenreich and H. R. Philipp, Phys. Rev. **128**, 1622 (1962).
[24] J. Tiggesbäumker, L. Köller, K. H. Meiwes-Broer, and A. Liebsch, Phys. Rev. A **48**, 1749 (1993).
[25] Y. Borensztein, W. L. Mochán, J. Tarriba, R. G. Barrera, and A.

Tadjeddine, Phys. Rev. Lett. **71**, 2334 (1993).
[26] V. Fernandez, D. Pahlke, N. Esser, K. Stahrenberg, O. Hunderi, A. Bradshaw, and W. Richter, Surf. Sci. **377**, 388 (1997).
[27] A. Zangwill and P. Soven, Phys. Rev. A **21**, 1561 (1980).
[28] N. D. Lang and W. Kohn, Phys. Rev. B **1**, 4555 (1970).
[29] M. Born and K. Huang, *Dynamical Theory of Crystal Lattices* (Oxford University Press, Oxford, 1988), Appendix of Chap. II.
[30] B. Persson and E. Zaremba, Phys. Rev. B **31**, 1863 (1985).